A design for a photonic syringe with multimode coupled slot waveguides

Zeno Gaburro

Dipartimento di Fisica, Università degli Studi di Trento, via Sommarive 14, 38100 Trento, Italy
gaburro@science.unitn.it

Abstract: A design is proposed that allows non-stationary field distribution with Bragg gratings in multiple slot waveguides. Selective coupling between modes is achieved or suppressed, according to controllable selection rules, based on mode symmetry. By applying such rules, *backward pulling* radiation pressure - i.e. toward the light source - can be obtained inside the slots. A mode-switching filter is also proposed, which allows the switching between forward and backward direction of radiation pressure. This "light-actuated" syringe could have potential applications for bidirectional particle trapping and manipulation, optofluidics, optomechanics and biotechnology.

OCIS codes: (130.3120) Integrated optical devices ;(230.0230) Optical devices; (230.1480) Bragg reflectors; (230.7370) Waveguides.

References and links

1. A. Ashkin, "Acceleration and Trapping of Particles by Radiation Pressure," Phys. Rev. Lett. **24**, 156-159 (1970).
2. A. Ashkin, "Optical trapping and manipulation of neutral particles using lasers," Proc. Natl. Acad. Sci. **94**, 4853–4860 (1997).
3. D. G. Grier, "A revolution in optical manipulation," Nature **424**, 810-816 (2003).
4. A. Yao, M. Tassieri, M. Padgett, and J. Cooper, "Microrheology with optical tweezers," Lab on a chip **9**, 2568-2575 (2009).
5. J. Nilsson, M. Evander, B. Hammarström, and T. Laurell, "Review of cell and particle trapping in microfluidic systems," Analytica Chimica Acta **649**, 141-157 (2009).
6. J. Pine, and G. Chow, "Moving Live Dissociated Neurons With an Optical Tweezer," IEEE Transactions on Biomedical Engineering 56, 1184 - 1188 (2009).
7. M. Murata, Y. Okamoto, Y. S. Park, N. Kaji, M. Tokeshi,and Y. Baba, "Cell separation by the combination of microfluidics and optical trapping force on a microchip," Analytical and Bioanalytical Chemistry **394**, 277-283 (2009).
8. R. D. Snook, T. J. Harvey, E. C. Faria, and P. Gardner, "Cell separation by the combination of microfluidics and optical trapping force on a microchip," Integrative Biology **1**, 43-52 (2009).
9. C. Brunner, A. Niendorf and J. A. Käs, "Passive and active single-cell biomechanics: a new perspective in cancer diagnosis," Soft Matter **5**, 2171–2178 (2009).
10. Y. Tsuboi, T. Shoji, M. Nishino, S. Masuda, K. Ishimori and N. Kitamura, "Optical manipulation of proteins in aqueous solution," Appl. Surf. Sci. **255**, 9906-9908 (2009).
11. S. Kawata and T. Tani, "Optically driven Mie particles in an evanescent field along a channeled waveguide," Opt. Lett. **21**, 1768-1770 (1996).
12. S. Kawata and T. Tani, "Optically driven Mie particles in an evanescent field along a channeled waveguide," Opt. Lett. **21**, 1768-1770 (1996).
13. D. J. Andrews, *Structured Light and its Applications*, (Elsevier, Amsterdam, 2008).
14. T. Tanaka and S. Yamamoto "Optically induced propulsion of small particles in an evenescent field of higher propagation mode in a multimode, channeled waveguide," Appl. Phys. Lett. 77, 3131 (2000).
15. G. Volpe, R. Quidant, G. Badenes, and D. Petrov, "Surface Plasmon Radiation Forces," Phys. Rev. Lett. 96, 238101 (2006).
16. G. Brambilla, G. S. Murugan, J. S. Wilkinson, and D. J. Richardson, "Optical manipulation of microspheres along a subwavelength optical wire," Optics Letters **32**, 3041-3043 (2007).

17. P. J. Reece, E. M. Wright, and K. Dholakia, "Experimental Observation of Modulation Instability and Optical Spatial Soliton Arrays in Soft Condensed Matter," Phys. Rev. Lett. **98**, 203902 (2007).
18. M. Righini, C. Girard, and R. Quidant, "Light-induced manipulation with surface plasmons," J. Opt. A: Pure Appl. Opt. **10**, 093001 (2008).
19. D. Neel, S. Getin, P. Ferret, M. Rosina, J. M. Fedeli, and O. G. Helleso, "Optical transport of semiconductor nanowires on silicon nitride waveguides," Applied Physics Letters **94**, 253115 (2009).
20. L. N. Ng, B. J. Luff, M. N. Zervas and J. S. Wilkinson, "Propulsion of gold nanoparticles on optical waveguides", Optics Communications **208**, 117-124 (2002).
21. K. Wang, E. Schonbrun, and K. B. Crozier, "Propulsion of Gold Nanoparticles with Surface Plasmon Polaritons: Evidence of Enhanced Optical Force from Near-Field Coupling between Gold Particle and Gold Film," Nano Letters **9**, 2623-2629 (2009).
22. S. Gaugiran, S. Gétin, J. M. Fedeli, G. Colas, A. Fuchs, F. Chatelain, and J. Dérouard, "Optical manipulation of microparticles and cells on silicon nitride waveguides," Opt. Express **13**, 6956-6963 (2005).
23. A. H. J. Yang, S. D. Moore, B. S. Schmidt, M. Klug, M. Lipson, and D. Erickson, "Optical manipulation of nanoparticles and biomolecules in sub-wavelength slot waveguides," Nature **457**, 71-75 (2009).
24. V. R. Almeida, Q. F. Xu, C. A. Barrios, and M. Lipson, "Guiding and confining light in void nanostructure," Opt. Lett. **29**, 1209–1211 (2004).
25. A. Jonas, and P. Zemanek, "Light at work: The use of optical forces for particle manipulation, sorting, and analysis," Electrophoresis **29**, 4813-4851 (2008).
26. E. Peral, and A. Yariv, "Supermodes of grating-coupled multimode waveguides and application to mode conversion between copropagating modes mediated by backward Bragg scattering," IEEE J. Lightw. Technol. **17**, 942 - 947 (1999).
27. R. Sun, P. Dong, N. Feng, C. Hong, J. Michel, M. Lipson, and L. Kimerling, "Horizontal single and multiple slot waveguides: optical transmission at λ = 1550 nm", Opt. Express **15**, 17967-17972 (2007).
28. L. Vivien, D. Marris-Morini, A. Griol, K. B. Gylfason, D. Hill, J. Álvarez, H Sohlström, J. Hurtado, D. Bouville, and E. Cassan, "Vertical multiple-slot waveguide ring resonators in silicon nitride", Opt. Express **16**, 17237-17242 (2008).
29. X. Tu, X. Xu, S. Chen, J. Yu, and Q. Wang, "Simulation Demonstration and Experimental Fabrication of a Multiple-Slot Waveguide," IEEE Photon. Technol. Letters **20**, 333-335 (2008).
30. C. Kittel, *Introduction to Solid State Physics*, 8th edition (Wiley, New York, 2004); N. W. Ashcroft and N. D. Mermin, *Solid State Physics* (Saunders College, Philadelphia, 1976).
31. M. L. Povinelli, M. Loncar, M. Ibanescu, E. J. Smythe, S. G. Johnson, F. Capasso, and J. D. Joannopoulos, "Evanescent-wave bonding between optical waveguides," Opt. Lett. **30**, 3042-3044 (2005).
32. F. Riboli, A. Recati, M. Antezza and I. Carusotto, "Radiation induced force between two planar waveguides", Eur. Phys. J. D **46**, 157-164 (2008).
33. J. Chan, M. Eichenfield, R. Camacho, and O. Painter, "Optical and mechanical design of a zipper photonic crystal optomechanical cavity," Optics Express 17, 3802-3817 (2009).
34. M. Li, W. H. P. Pernice, and H. X. Tang, "Tunable bipolar optical interactions between guided lightwaves," Nature Photonics **3**, 464-468 (2009).
35. P. B. Deotare, M. W. McCutcheon, I. W. Frank, M. Khan, and Marko Lončar, "Coupled photonic crystal nanobeam cavities," Appl. Phys. Lett. **95**, 031102 (2009).
36. C. R. Pollock, *Fundamental of optoelectronics* (Irwin, 1994); B. E. A. Saleh and M. C. Teich, *Fundamentals of Photonics* (Wiley, New York, 1991).
37. E. D. Palik, *Handbook of Optical Constants of Solids, Volume 3* (Academic Press, 1997).
38. P. Barthelemy, M. Ghulinyan, Z. Gaburro, C. Toninelli, L. Pavesi, and D. S. Wiersma, "Optical switching by capillary condensation," Nature Photonics **1**, 172-175 (2007).

1. Introduction

Research into trapping and manipulation of particles by propagating electromagnetic fields has been active for almost four decades [1] and has led to a large number of applications [2,3] particularly in microfluidics, biology and medicine [4-10]. More recently, particle trapping and propulsion by evanescent electromagnetic fields has also been achieved [11,12]. For manipulation, evanescent fields offer many advantages over free space beams, including background signal reduction, and large-scale manipulation of thousands of particles in parallel [13]. Evanescent fields for trapping and propulsion of dielectric particles [11,12,14-18], semiconducting particles [19], metallic particles [12,20,21], cells [22] and biomolecules [23] can be obtained, by exploiting total internal reflection (TIR) in prisms [11,17] and in waveguides [12,14,16,20], or surface plasmon-polaritons (SPPs) [15,18,21]. In highly sub-wavelength waveguides, trapping is particularly effective because almost all the optical energy is carried by evanescent fields [16]. In SPP waveguides, one can take advantage of field enhancement associated with plasmonic resonances [21]. On the other hand, in dielectric slot waveguides [24], the strength of the optical force can be enhanced by confining the electromagnetic evanescent fields [23]. Further applications of optical forces due to evanescent fields include nonlinear optics [17], optofluidics [22] and nanobiotechnology [25].

Because they are exponentially decaying, evanescent fields always exhibit intensity gradients, which result in gradient forces. The effect of these forces is to pull the particles toward the interface that sustains the evanescent wave. However, the wave also exerts a force on the particles due to radiation pressure. This force originates from the scattering of the field by the particle. The net scattering force pushes particles along the direction of propagation of the beam [3].

In this paper, I suggest a multimode waveguide design which supports backward (i.e., toward the source) propagating modes with substantial evanescent fields. With this design, the direction of propagation can be flipped by changing the mode of injection. Propulsion of particles can be therefore also inverted in direction.

2. Signature of supermodes in coupled slot waveguides

If a waveguide supports at least two modes, non-stationary field distributions can be achieved by reflection. Let us consider a waveguide with two modes, whose propagating constants are β_0 and $\beta_1=\beta_0+\Delta\beta$. The signs of β_0 and β_1 are opposite if they are counter propagating. Let us now suppose that electromagnetic energy, initially travelling in mode β_0 only, is reflected from mode β_0 to backward mode β_1. This reflection leads to non-stationary field distribution, because the field profiles of mode β_0 and β_1 are necessarily different, since they belong to different modes. Such reflection could be due, for example, to a photonic structure with period

$$\Lambda = \frac{2\pi}{|\Delta\beta|}. \tag{1}$$

The coupling of different counter propagating modes in multimode waveguides has been already suggested for mode conversion, but, to the author's knowledge, without an explicit waveguide design, nor discussing applications for optomechanics [26].

The condition in Equation 1 is a constrain on the period, but gives no hint about how to design the unit cell of the photonic structure. Here, a possible procedure is suggested, which utilizes coupled slot multimode waveguides. Coupled slot waveguides have been already demonstrated, both in horizontal [27] and vertical [28,29] configurations for single mode guiding but, to the author's knowledge, not for multiple mode guiding.

In this work, a multiple n-slot waveguide is considered, which is composed by n+1 coupled homogeneous and equal waveguides. The idea for the design is inspired by the tight-binding method, a very useful approximation in atomic and chemical physics not only to simplify the calculations, but also to gain deeper insight into electron states in complex molecules and crystals [30]. In the tight-binding procedure, molecular or crystalline orbitals are described as linear combinations of atomic orbitals (LCAO). The analogy between coupled waveguides and molecular orbitals has been already proposed for calculating transverse optomechanical forces between coupled waveguides [31-35]. In the case of waveguides, the uncoupled picture, corresponding to isolated atoms, is the set of all the separate n+1 waveguides, considered at infinite distance from each other. The modes of the separate waveguides are the analogous to atomic orbitals. When these elementary components are brought closer together, the coupling of elementary eigenmodes lifts the degeneracy of the originally degenerate supermodes (i.e. the modes of the whole waveguide, considered as a single entity).

Let us first recall the main ideas of the tight binding approximation for the electronic case. For crystalline orbitals, the electronic wave functions $\psi(\mathbf{r})$ are solutions of an eigenvalue equation (Schrödinger equation) in a periodic potential. Because of the latter condition, the problem possesses translational symmetry, thus the wave functions must satisfy the Bloch theorem. On the other hand, the wave functions $\psi(\mathbf{r})$ should retain a trace of the wave functions $\psi_n(\mathbf{r})$ of isolated atoms, at least when the atomic distance is not too close, in some sense. This assumption is the core of the tight binding method. Without loss of generality, an eigenfunction $\psi(\mathbf{r})$ can both satisfy the Bloch theorem and be expressed in terms of functions $\varphi(\mathbf{r})$ (Wannier functions) centered at atomic sites in the lattice, as [30]

$$\psi_{\mathbf{k}}(\mathbf{r}) = \sum_{\mathbf{R}} e^{i\mathbf{k}\cdot\mathbf{r}} \phi(\mathbf{r}-\mathbf{R}), \tag{2}$$

where $\mathbf{R}$ is a lattice vector, and the Bloch wave vector $\mathbf{k}$ has also been used to label the eigenfunction. The isolated atomic wave functions can be introduced by expanding the Wannier functions as

$$\phi(\mathbf{r}) = \sum_{n} b_n \, \psi_n(\mathbf{r}), \tag{3}$$

where the b_n's are the required expansion coefficients. Generality of Equation 3 is guaranteed by the completeness of the eigenset $\{\psi_n\}$. At this point, in the tight binding approximation, one looks for the conditions for the Equation 3 to be approximately true with few, possibly only one, $\psi_n(\mathbf{r})$. These conditions can be expressed as the vanishing of overlap integrals, given the target wave function $\psi_n(\mathbf{r})$, with all the wave functions $\psi_m(\mathbf{r})$ [30]

$$\int \psi_n^*(\mathbf{r})\, \psi_m(\mathbf{r}-\mathbf{R})\, \mathrm{d}\mathbf{r} \ll 1 \quad (\text{for } \mathbf{R} \neq 0), \quad \text{and} \quad \int \psi_n^*(\mathbf{r})\, \Delta U(\mathbf{r})\, \psi_m(\mathbf{r}-\mathbf{R})\, \mathrm{d}\mathbf{r} \ll 1, \tag{4}$$

where ΔU is the difference between the crystalline and the single atom potential.

This approximation can be extended to waveguide modes. The expansion in Equation 3 requires the completeness of the eigenmode set, thus in principle all unguided modes must also be included. But, as before, the question is under what conditions it is possible to build a supermode as a superposition of few (possibly only one) displaced elementary guided modes. The conditions can be formulated similarly to Equations 4. The Schrödinger equation must be substituted with the Helmholtz equation for the modes of waveguides, which reads (assuming scalar form)

$$\nabla^2 E + k_0^{\,2} n_c(\mathbf{r})^2 E = 0, \tag{5}$$

where E is the amplitude of the electric field, k_0 is the magnitude of the wave vector, and $n_c(\mathbf{r})$ is the refractive index as a function of space. Equation 5 implies that the term ΔU must be substituted by a term $k_0^2[n_c(\mathbf{r})^2\text{-}n_s^2]$, where n_s is the refractive index of the background, and the integral can be limited to waveguide cores, because outside the cores n_c=n_s. For the overlap integrals to be small, ultimately, Equations 4 require the decay length of evanescent field of the target mode to be small compared to the distance of waveguides.

For this paper, the tight-binding picture is primarily useful to introduce the *signature* of supermodes' profile of the electric field. The concept of the signature can be outlined as follows. Let us assume for simplicity that the problem is two dimensional (i.e., that the elementary waveguides are slabs), and that the distance d between nearest neighboring elementary waveguides is the same for all the waveguides, and is large enough for a mode of elementary waveguides to satisfy the conditions in Equation 4. Let us indicate with $f_e(y\text{-}md)$ the (real valued) profile of the electric field of this mode, in the m^{th} elementary waveguide, where y denotes the transverse coordinate. The origin of y is taken to be the middle point of transverse cross section of first waveguide (slab 0). Let us also indicate with $f_h(y)$ the field profile of supermode h of the whole waveguide. In the limit of $n \to \infty$, the structure is periodic. Hence, according to Equation 2, the real-valued $f_h(y)$ can be approximately expressed as a quasi-Bloch function as

$$f_h(y) \approx C \sum_{m=0}^{m=n} \cos(K_h\ y)\ f_e(y - md), \tag{6}$$

where C is a normalization constant, and $K_h = h\pi/nd$ (for $h=0, 1, ..., n$). In Equation 6, by referring to a discrete set of K_h, I contextually introduced also the quantization of K_h, which is a consequence of the finite extension of the system in the y coordinate. The parameter h individuates all the $n+1$ wave vectors, in the first Brillouin zone, relative to the $n+1$ supermodes.

By applying the assumptions of the tight binding approximation, I assume that $f_e(y\text{-}md)$ essentially vanishes in proximity of the neighboring waveguides, or $f_e(y\text{-}md) \neq 0$ only for $y \approx md$ (on the scale of d), which leads to

$$f_h(y) \approx C \sum_{m=0}^{m=n} \cos(h\pi m / n)\ f_e(y - md). \tag{7}$$

From Equation 7 one can define the "signature" of supermode h as the set of the signs of the $n+1$ coefficients $\cos(h\pi m/n)$. For a given set on n+1 elementary waveguides, there are n+1 signatures, each being characterized by the number of sign changes. The sign can change up to n times. For each supermode, this number is described by parameter h. Hence, it is the magnitude of the Bloch wave vector which determines the number of sign changes in the signature. An example is given in Figure 1, where the number of slots is n = 2, the number of elementary waveguides is n+1=3, and hence the signatures are (+++) for h=0, (+0-) for h=1, and (+-+) for h=2.

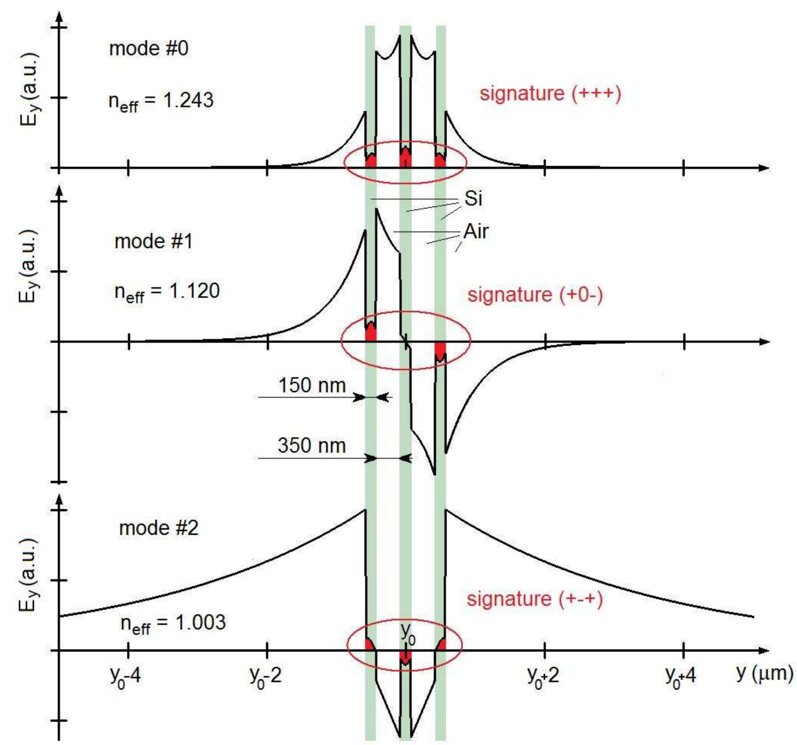

Fig. 1. Signatures of the 3 guided TM supermodes at vacuum wavelength λ_0=1.55 μm in a 2-slot waveguide resulting from 3 coupled 150 nm thick Si slabs. Air slots are 350 nm thick. For each supermode, the effective index n_{eff} is also shown. The thickness of Si slabs is chosen to guarantee single mode operation (for the isolated slab).

Thus, the signature of supermodes can be associated to the "dominant sign" of the field profile across the elementary waveguides. The definition is suggested by Equation 7 under quite strict assumptions, but the example in Figure 1 shows that its physical meaning can be robust even in cases for which the coupling is not weak, or n is very small ($n=2$, in Figure 1). In general, however, one must be careful in evaluating the signature according to Equation 7. This especially applies to slot waveguides: to the take full advantage of the field enhancement in the slots, deeply sub wavelength slot size is required, i.e. strong waveguide coupling. In such case, supermodes cannot be accurately described with tight-binding approximation. Moreover, when n is small, boundary effects can acquire larger importance, and thus the profile of supermodes can deviate significantly from a Bloch function. For these reasons, it is helpful to provide an operative extension of the definition of supermode signatures. A practical way can be the following. First, one analytically [24] or numerically [36] calculates the actual field profile $f_h(y)$ of each supermode. The sign of the m^{th} coefficient in the signature of supermode h can be again associated to the "dominant sign" of the m^{th} waveguide, which can be now defined as the sign of an integral of the type

$$\int_{a(m)}^{b(m)} f_h(y)dy, \tag{8}$$

where $a(m)$ and $b(m)$ are the boundaries of the m^{th} elementary waveguide. A definition with the integral in Equation 8 resolves the issues related to the assumptions for Equation 7.

Once the signature is known, the design of mirrors which couple different supermodes can be performed by considering the required operation on single signs in the signature. Let us apply this idea, for example, to the mentioned case of the 2-slot waveguide of Figure 1, with the goal of coupling, by reflection, supermode +++ to supermode +-+. There are two ways to perform this sign change. The first is by maintaining the sign of the first and last coefficients, and flipping the sign of the central coefficient. The second is by flipping the first and last sign, and maintaining the central sign unaltered (signature -+- is the same signature as +-+). The change or maintenance of sign in each elementary reflection can be achieved according to Fresnel reflection coefficient r, which, for normal incidence, reads

$$r = \frac{n_0 - n_1}{n_0 + n_1}, \tag{9}$$

where n_0 (n_1) is the refractive index of the medium of incidence (refraction). Thus, there is a 0 (π) phase shift in the reflected beam, if the medium of incidence has higher (lower) index than the medium of refraction. Equation 9 also holds for effective indices $n_{eff}=|\beta c/\omega|$ in a waveguide, where c is the speed of light in vacuum, and ω is the angular frequency [36]. In a waveguide, the effective index increases with increasing the core thickness. Hence, a reflection without (with) a change of sign, in a waveguide, can be obtained by an abrupt thinning (thickening) of the waveguide core, as this implies an abrupt decrease (increase) of the effective index n_{eff} (Figure 2).

3. Two dimensional design and finite-difference time-domain simulation

Because of the phase relationships in the individual slabs, the structure in Figure 2 is expected to efficiently couple supermode +++ to supermode +-+ with opposite propagation, and vice versa. The conditions for the largest reflection in a 1D Bragg mirror, fabricated by alternating layers with low (high) refractive index n_l (n_h) and thickness d_l (d_h), read

$$d_l = \frac{\lambda_0}{4n_l} \text{ and } d_h = \frac{\lambda_0}{4n_h}, \tag{10}$$

where λ_0 is the vacuum wavelength. Equations 10 can be interpreted as the conditions to get a π phase shift in a roundtrip in any of the layers.

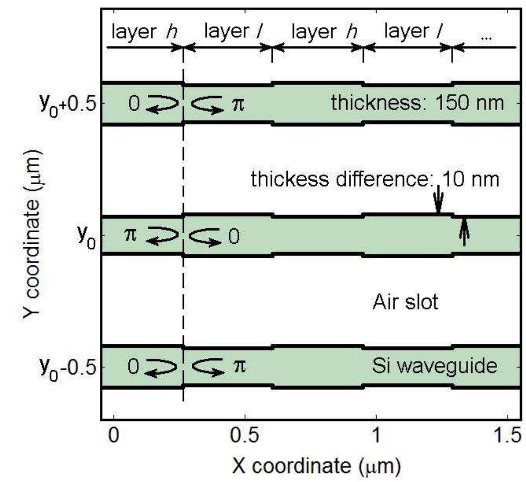

Fig. 2. Photonic structure to reflect supermode +++ to supermode +-+ (see Figure 1). The dashed line indicate one of the reflecting interfaces. The phase shift associated to elementary reflections is shown by bending arrows. The period Λ of the structure (690 nm) and the other values are resulting from the procedure described in the text. Layer *h* (higher effective index) and layer *l* (lower effective index) refer to the 2 types of quasi-1D layers which define the Bragg mirror. The graph is to scale.

I generalize this condition of a π phase shift per roundtrip by assuming that forward and backward propagation are carried out in different supermodes. Thus, even in the same layer, there are two different refractive indices, one for the forward and one for the backward direction. Moreover, a Bragg mirror has two kinds of "layers". For example, in Figure 2, the layers are identified by the thickness of the three slabs (layer *h*: thick-thin-thick, and layer *l*: thin-thick-thin). Therefore, there are 4 relevant refractive indices, which I label here as $n_{(i,j)}$, where *i* indicates the layer type (*i*=*h* or *l*), and *j* the direction, forward or backward (*i*=*f* or *b*). Equations 10 are therefore generalized as

$$d_l = \frac{\lambda_0}{2\,(n_{l,f} + n_{l,b})} \text{ and } d_h = \frac{\lambda_0}{2\,(n_{h,f} + n_{h,b})}. \tag{11}$$

An additional simplification has been introduced in Figure 2, by imposing the corrugation to be small with respect to the thickness. This condition limits the mode mismatch - hence, unwanted mode mixing - between layers of type *h* and *l* layers. Small corrugation implies small index contrast, and thus, from Equations 11, $d_l \approx d_h$. The calculated value is $d_l \approx d_h \approx 345$ nm, thus the period Λ is 690 nm (Figure 2).

Once the period has been defined, just because of the periodicity, additional stop bands are expected to appear in the transmission spectrum. Their central wavelength can be estimated by solving Equations 11 for λ_0, by inserting the now known values of d_l and d_h, and all the meaningful combinations of refractive indices. For example, a stop band is expected which reflects supermode +++ to itself. Its central wavelength can be estimated as follows. The numerically calculated effective index of supermode +++ is approximately 1.209 at $\lambda_0 \approx 1.7$ μm (note that the value 1.243 in Figure 1 is calculated at 1.55 μm). The estimated central wavelength of the +++ to +++ stop band is $\lambda_0 = 4n_l d_l = 1.668 \pm 0.024$ μm (the error is added assuming a 10 nm tolerance for d_l).

Two 2D FDTD simulations of the structure in Figure 2 with 100 periods have been performed using commercial software (FDTD Solutions by Lumerical Solutions, Inc.). The purpose of the first simulation is the spectral characterization. Hence, a broadband source has been used as stimulus. The injected field had the beam profile of supermode +++ in Figure 1, a central wavelength $\lambda_0 = 1.6$ μm, and a full width at half maximum of $\Delta\lambda \approx 400$ nm. The geometrical mesh had 10 nm and 5 nm step size resolution, respectively, in x and y directions. The total span of the simulation region in the x direction was determined by the structure itself, whereas in the y direction was set to 20 μm, to simulate the evanescent tails with satisfactory approximation. The material (Si) was simulated by taking into account both real and imaginary part of permittivity according to Palik [37]. The time step was 99% of Courant stability limit. The results are shown in Figure 3.

The effectiveness of the design is demonstrated by presence of the stop band at 1.545 μm (supermode +++ reflected to supermode +-+, inset a in Figure 3), and simultaneously by the almost complete suppression of the stop band at 1.645 μm (supermode +++ to itself, inset c in Figure 3). The location of the latter is consistent with the previously estimated 1.668±0.024 μm. The suppression cannot be ascribed to a low index contrast, which would also similarly affect the band at 1.545 μm. Instead, suppression is due to the symmetry mismatch between the signatures of the modes.

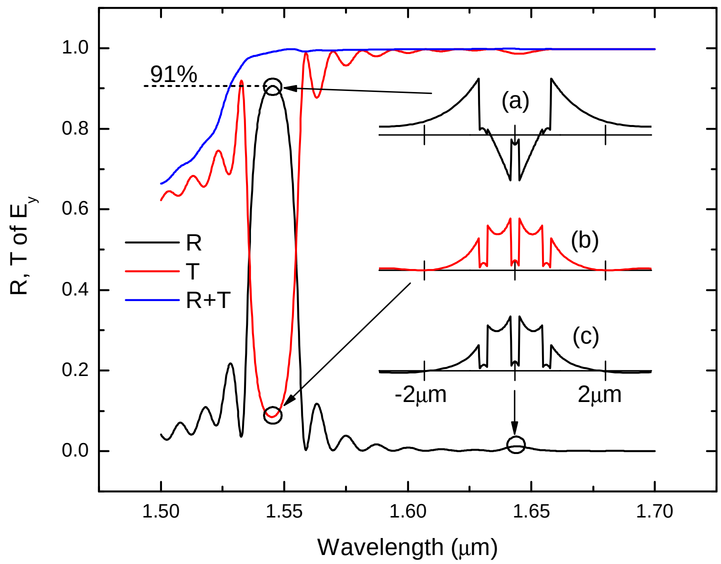

Fig. 3. 2D FDTD simulation of transmission and reflection spectra of the structure in Figure 2 with 100 periods and with supermode +++ excitation (see Figure 1). The stop band is relatively narrow due to the low contrast of effective refractive index. Insets show the profile of electric field E_y. In (a), the reflected beam has the profile of supermode +-+, whereas in (c) the profile of reflected beams matches the profile of incident beam (not shown), as expected, because the Bragg condition is satisfied for the reflection from supermode +++ to itself. However, in (c), reflection is *almost completely suppressed by the symmetry mismatch of the mirror* (residual reflection is ≈1.2%). Inset (b) shows that the transmitted beam maintains the profile of supermode +++. Decrease of R+T at lower wavelength is due to coupling by the grating of supermode +-+ to free space propagation.

One can picture this suppression as a *selection rule*, dictated by symmetry, in close analogy with rules that prevent transitions between electronic states due to symmetry constrains. In such analogy, backward (forward) modes can formally be assimilated to "bra" <+++| ("ket" |+++>) vectors, and the mirror to an "operator" |+-+|. The "matrix element" <+++|+-+|+++> approximately vanishes, whereas <+-+|+-+|+++> encodes the information of the "oscillator strength" of a single interface. The value can be calculated, analytically, from overlap integrals of modes, or numerically from simulations, as the ratio between the integral of reflected field versus the integral of incident field. However, this is not further investigated in this work. Instead, I suggest that this notation can be directly exploited: the vanishing or non-vanishing character of matrix elements can be obtained as the straightforward result of sign multiplications. In the two sample cases above, the sign multiplications yield (+-+) and

(+++), respectively. The presence of the minus sign in the first case indicates a symmetry forbidden transition, hence a vanishing matrix element.

The second simulation was performed with similar FDTD settings, except that a narrowband instead of broadband source was used. The wavelength 1.545 μm was chosen for this simulation: at this wavelength, the stop band that generates the backward propagation effect has a maximum (Figure 3). For this simulation, the excitation source was set to supermode +-+, to obtain backward reflection to supermode +++. This choice leads to backward propagation of the evanescent *slot-confined* field, which is more interesting for the applications. The companion spectrum (forward propagating supermode +-+ and back reflection to supermode +++, not shown) does not deviate significantly from the spectrum in Figure 3.

A snapshot of the resulting 2D map of Poynting vector over a few periods, close to the input end of the waveguide, is shown in Figure 4.

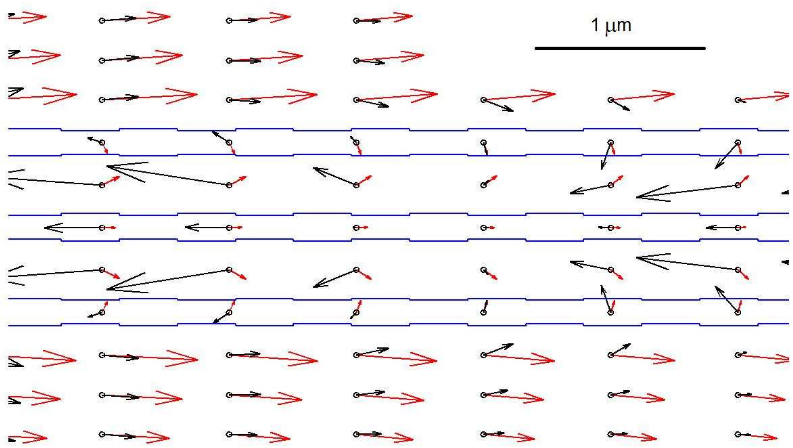

Fig. 4. 2D FDTD simulation of Poynting vector of the structure in Figure 2, with 100 periods, and with supermode -+- excitation (see Figure 1). Light injection is from the left side. Excitation is narrowband (vacuum wavelength $\lambda_0 \approx 1.54$ μm). Map is to scale. Only a few periods are shown, in proximity of the input side. Red (black) arrows show the result without (with) corrugation. The blue lines are the outline of the structure with corrugation. While the energy in the outer side of the waveguide is always traveling forward (top and bottom of figure), in the slots (i.e. in the 2 regions between the slabs), the component along the waveguide axis is dominantly forward (backward) in absence (presence) of the corrugation.

The steering effect of the structure can be clearly seen looking at the black arrows, which are the calculated Poynting vectors from the FDTD outputs (red arrows show the result of simulation with no corrugation on the waveguides). The black vectors initially point to the right (top left and bottom left of the figure, outside the slots and of the waveguide structure). This direction is outward with respect to the source (which is located at the left, out of the shown region). Moving to the right, black arrows start turning toward the center of the structure. In the core of outer waveguides, the vectors keep being directed toward the center of the structure (right side of figure), but they also acquire negative component in the x direction. Finally, in the two slots, the x component is negative almost in every sampled point considered. The backward effect is the net result of the fields of backward supermode +++ and of forward supermode +-+. The key idea is that, *in the slots*, the amplitude of the latter is lower. A snapshot of the movie of the simulation of electric field E_y (Media 1) is shown in Figure 5.

4. Switching of the direction of radiation pressure

The direction of radiation pressure can be switched by switching the supermode of injection. In fact, the direction of the radiation pressure in the slots depends on the direction of propagation of supermode +++. If the injection is directly in supermode +++, the radiation pressure in the slots will be trivially outward (away from the source). However, if the injection is in supermode +-+, this supermode will be back reflected by the structure to supermode +++, and the pressure will be directed toward the source in the slots. In this section, I propose a sample device (Figure 6) to switch the mode of injection. This structure is meant to be placed before the main device of Figure 2.

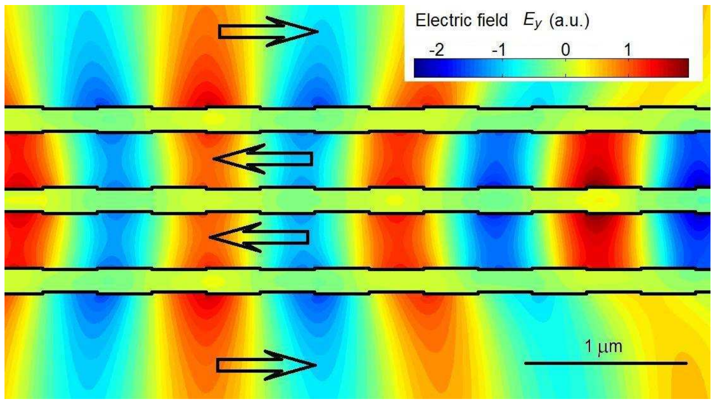

Fig. 5. Snapshot of the electric field E_y distribution, according to 2D FDTD simulation of the structure in Figure 2, with 100 periods, and with supermode -+- excitation (see Figure 1). Light is injected from the left side. Excitation is narrowband (vacuum wavelength $\lambda_0 \approx 1.54$ μm). Only a few periods are shown, in proximity of the input side. Map is to scale. Large arrows indicate the direction of energy flux (Media 1).

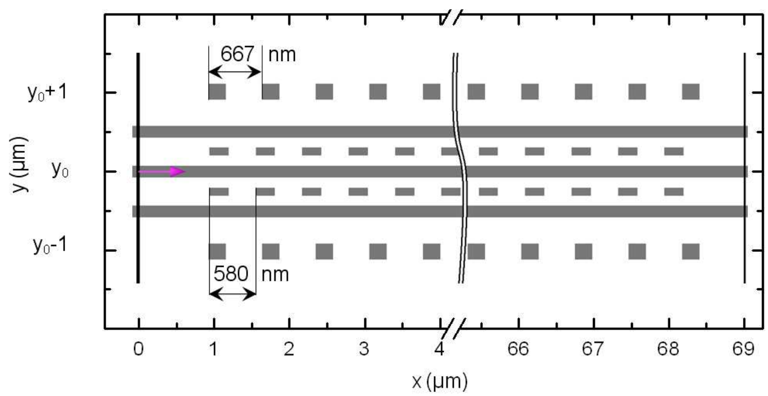

Fig. 6. Sample 2D photonic structure to selectively filter supermode +++ or supermode +-+ (supermode profiles are shown in Figure 1). Grey (white) areas represent Si (air). The vertical line at x = 0 μm indicates the location of the energy source in FDTD simulations. The arrow indicates the direction of injection. The vertical line at x = 69 μm indicates the location of monitor. The graph is to scale.

The backbone of the device in Figure 6 is the set of three coupled waveguides shown in Figure 2, however in this case the waveguides have no corrugation. Instead, two photonic structures are added. The idea is to take advantage of two *independently* designed band structures. The first structure is constituted by the rows of thinner rectangles inside the slots, and is designed to generate a stop band to reflect supermode +++ to itself. Its period (580 nm) locates the *lower-wavelength* band-edge of the stop band slightly below 1.545 μm (i.e. the wavelength for which backward effect in the main device is largest, see Figure 3). A FDTD simulation of the device in Figure 6, under excitation of supermode +++, is shown as a black curve in panel a of Figure 7. This figure demonstrates that this first photonic structure acts as a "closed gate" for supermode +++ at 1.545 μm (black dot, transmission is T_c≈0.1%). However, a relatively small red shift of the spectrum can open this gate, and let the supermode pass. This situation is simulated in panel b of Figure 7, where the refractive index of the background has been increased by 2%. The transmission of supermode +++ (black line) increases to about T_o≈49% (black dot in panel b). In this "open gate" configuration, the insertion loss is about 3 dB, whereas the modulation depth $(T_o-T_c)/(T_o+T_c)$ is larger than 99%. There are several possible options to achieve experimentally a shift that is compatible with this simulation. For example, if the background is a controlled fluid, the shift can be obtained by changing the composition of the fluid. If the structure is porous, a more subtle way could be by resorting to capillary condensation, as we have already demonstrated experimentally in a different context [38]. Other solutions could include nonlinear materials.

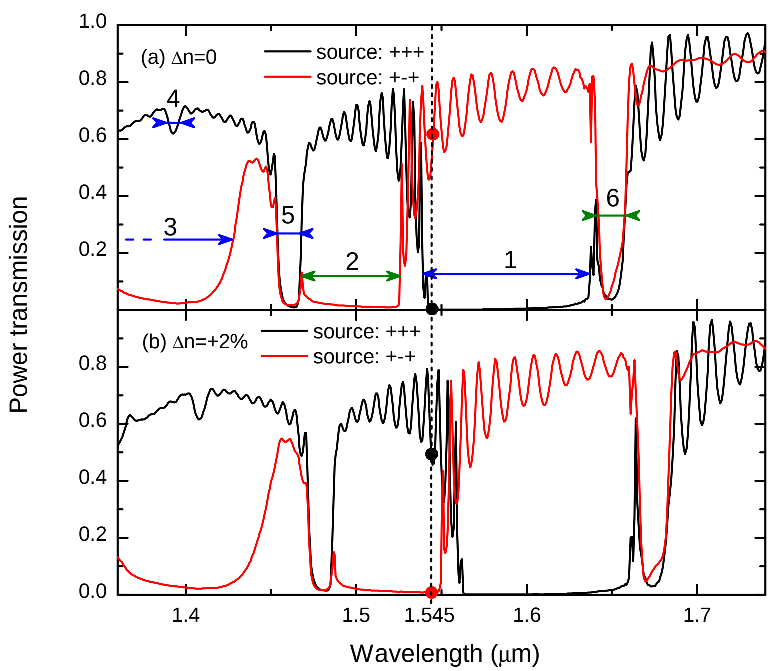

Fig. 7. 2D FDTD simulation of transmission spectra of the structure in Figure 6. Each spectrum has been calculated by exciting only one supermode. Black (red) curve is the relative power transmission of supermode +++ (supermode +-+). The refractive index of Si was modeled as a complex quantity according to Palik [37] (the real part at 1.545 μm was about 3.48). Panel a shows the simulation with the background refractive index set to $n_0 = 1$. Panel b shows the simulation with an increase of the background index by 2%. The vertical dashed line is the design wavelength for this filter (1.545 μm). Colored dots indicate the transmission of the supermodes at this wavelength. In panel a (b), the power transmission is 0.1% (0.8%) for supermode +++ (supermode +-+), and about 57% (49%) for supermode +-+ (supermode +++). The bands generated by the photonic structure with period 580 nm (667 nm) are marked by blue (green) arrows. Band 1 reflects supermode +++ to +++, band 2 supermode +-+ to +-+, band 3 supermode +-+ to +-+, band 4 is the same as band 3, but occurs under excitation with supermode +++ due to stray coupling with supermode +-+. Band 5 (band 6) appears in both the red and black curve because it is couples supermode +++ to supermode +-+ and it is provided by the inner (outer) photonic structure.

In similar fashion, the second photonic structure is placed in the space outside (two rows of thick rectangles in Figure 6). In this case, the period (667 nm) is designed to introduce a stop band for supermode +-+, with the *upper-wavelength* band-edge slightly below 1.545 nm. In Figure 7, the FDTD simulation, under excitation of supermode +-+, is shown as a red curve. As opposed to the previous case, in absence of spectral shifts this photonic structure acts as an "open gate" (transmission is T_o≈57%) for supermode +-+. A relatively small red shift of spectrum closes the gate and blocks the supermode +-+. This blocking effect is demonstrated in panel b of Figure 7 (red curve). Transmission drops to about T_c≈0.8%, and modulation depth $(T_o$-$T_c)/(T_o+T_c)$ in this case is about 97%. Incidentally, the first photonic structure, although designed for supermode +++, unavoidably introduces a stop band also for supermode +-+ (visible in Figure 7, band 3). However, this band has no relevant effect for this design because it is located away at lower wavelength (this is due to the lower effective index of supermode +-+). On the other hand, the second photonic structure has no observable effect at all, on supermode +++. In fact, in this case, additional bands are suppressed, due to the negligible overlap in space between the second structure and supermode +++.

Finally, to excite both +++ and +-+ supermodes simultaneously, the structure of Figure 6 was excited only in the central waveguide (left panel of Figure 8). The output of the device is shown in the central panel of Figure 8.

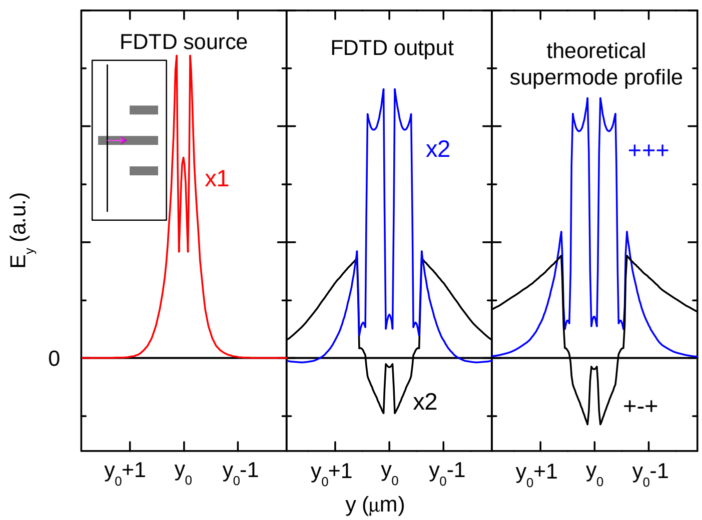

Fig. 8. 2D FDTD simulation of simultaneous excitation of supermodes +++ and +-+ in the device in Figure 6. Left panel: field profile of source (the central waveguide in Figure 6 has been prolonged to the left, as shown in the inset, to allow this mode profile). Simultaneous excitation is due to mismatch between the source and the supermodes profiles. Central panel: field profile of the output, with no index shift (black curve) and with 2% shift (blue curve). Right panel: analytical profile of the +++ (blue curve) and +-+ (black curve) supermodes. Comparison between the central and the right panel shows that the output of the device has a field profile almost overlapping a single supermode (either +++ or +-+), depending on the index of the background. Hence, the structure in Figure 6 works as a supermode selector. Residual components of the other modes are observable as deviations from the theoretical profile (particularly visible for $|y$-$y_0|$>1 μm).

Without any index shift, only the supermode +-+ passes through. This supermode, injected in the device of Figure 2, leads to the backward propagation effect in the slots. If on the other hand the refractive index is shifted by 2%, then only the supermode +++ passes through, and the radiation pressure will be directed forward.

6. Conclusions

Multimode coupled slot waveguides can be structured for selective mode coupling. Selection of modes can be achieved by exploiting the symmetry of modes. For example, a distributed Bragg mirror has been proposed, which reflects a mode to a different one. The design presented here takes advantage of a generalization of the well known "$\lambda/4$ optical thickness" rule for the layers of distributed Bragg mirrors. Finite-difference time-domain simulations show that stop bands obtained with this generalized procedure can appear or be suppressed, according to consistent selection rules, which are reminiscent of selection rules for eigenmodes transitions in quantum mechanics. As an intriguing application, I have proposed a design of slot waveguides, in which backward pulling radiation pressure could be obtained in evanescent fields inside the slots. Furthermore, I have also suggested a front-end filter that can allow the switching between forward and backward direction of this radiation pressure. The integration of the front-end filer with the backward-wave device could behave as a syringe, in which the "needle" is constituted by the corrugated empty slots, thus naturally suggesting potential applications as a tool for biotechnology.

Acknowledgments

The author gratefully acknowledges the School of Engineering and Applied Science (SEAS) at Harvard University for providing the simulation facilities, Prof. F. Capasso for his support, and all the members of his group for fruitful discussions and help with the FDTD simulations, especially M. A. Kats, R. Blanchard and J. Fan. The research leading to these results has received funding from the European Community's Seventh Framework Programme (FP7/2007-2013) under grant agreement n° PIOF-GA-2009-235860.